Equivariant Parameter Sharing for Porous Crystalline Materials

Marko Petković[1,2][0009−0000−4918−6027], Pablo Romero Marimon[1][0000−0001−9164−6541], Vlado Menkovski[1,2][0000−0001−5262−0605], and Sofia Calero[1,2][0000−0001−9535−057X]

[1] Eindhoven University of Technology, Eindhoven, The Netherlands
{m.petkovic1, v.menkovski, s.calero}@tue.nl
p.romero.marimon@student.tue.nl
[2] Eindhoven Artificial Intelligence Systems Institute, Het Kranenveld 12, Eindhoven, The Netherlands

Abstract. Efficiently predicting properties of porous crystalline materials has great potential to accelerate the high throughput screening process for developing new materials, as simulations carried out using first principles model are often computationally expensive. To effectively make use of Deep Learning methods to model these materials, we need to utilize the symmetries present in the crystals, which are defined by their space group. Existing methods for crystal property prediction either have symmetry constraints that are too restrictive or only incorporate symmetries between unit cells. In addition, these models do not explicitly model the porous structure of the crystal. In this paper, we develop a model which incorporates the symmetries of the unit cell of a crystal in its architecture and explicitly models the porous structure. We evaluate our model by predicting the heat of adsorption of CO_2 for different configurations of the mordenite zeolite. Our results confirm that our method performs better than existing methods for crystal property prediction and that the inclusion of pores results in a more efficient model.

Keywords: Graph Neural Networks · Porous Materials · Symmetries.

1 Introduction

Deep Learning has shown to be of great use in materials science, in tasks like property prediction and high-throughput screening of potential materials [5]. In these workflows, many materials are first simulated using first principles methods, such as Density Functional Theory (DFT) and classical simulation, such as Molecular Dynamics (MD), to find candidate materials to synthesize. However, these simulations are often computationally expensive and can take days or weeks to simulate a single new material. With Deep Learning, it is possible to accelerate the process of finding suitable materials, by developing data-driven surrogate models. These models scale significantly better than first principle simulators and allow for efficient search of the space of potential candidates [27].

Graph Neural Network (GNN) architectures are commonly used for modeling molecules and materials [22] as these objects can effectively be represented as a graph. However, general-purpose GNNs are too restrictive as they incorporate only a part of the symmetries and periodicity present in crystal structures.

To overcome these limitations, for crystalline materials, multiple GNN architectures have recently been proposed [2,4,16,24,31,32] that accurately predict the properties of materials. These methods are specific extensions of general-purpose GNN that preserve the geometric structure of the crystal in their data representation. Despite preserving the geometric structure, none of the proposed models explicitly encode any information regarding pores, as the empty space does not lie on the data domain, and is thus not taken into account. Furthermore, they do not make use of the crystal symmetries in the material representation, since they are typically equivariant to a symmetry group larger than the space group of the crystal. We hypothesize that model architectures that do not explicitly model the porous structure of porous materials will struggle to infer the relevance of atom arrangements around pores for different properties.

Zeolites are a type of porous, crystalline materials of particular interest, as they are easily synthesizable [17]. They are used in applications such as gas separation and are a potential method for carbon capture [26]. The crystal structure of zeolites consists of TO_4 tetrahedra. In these tetrahedra, the T-atoms can either be aluminium or silicon, and both have different influences on the properties of the material. All four corners of the tetrahedra are shared, which results in a porous material. In Figure 1a, the porous structure of the Mordenite (MOR) and ZSM-5 (MFI) zeolites can be seen. The ability to capture CO_2 of a zeolite can be measured by its heat of adsorption in kJ/mol and is calculated as follows: $-\Delta H = \Delta U - RT$. Here, ΔU is the difference in internal energy before and after adsorption, R is the universal gas constant, and T is the temperature. The heat of adsorption can be influenced by the structure of the different types of zeolites and the amount and distribution of aluminium atoms in the framework [3,19,33].

Due to the difference in charge between aluminium and silicon atoms, it is necessary to balance the charge when aluminium atoms are present in a framework. To achieve this, cations such as sodium are inserted in the crystal structure. Since the cations are positively charged, they additionally attract CO_2 through Coulombic forces, thus increasing the ability of the material to adsorb CO_2. However, while the cations increase the adsorption strength, they also occupy physical space in the pores of the material. When multiple sodium cations are inside a pore, they can restrict CO_2 from entering it. As a result, the adsorption capacity of the material decreases. It is unclear which distributions of aluminium and silicon in different zeolites are optimal to maximize the heat of adsorption.

In this paper, we propose a novel GNN architecture that exploits information regarding the porous structure, as well as the symmetry of these materials, using parameter-sharing based on their space groups. This model allows us to effectively model the properties of porous crystalline materials.

We empirically validate our approach by modeling the heat of adsorption of CO_2 for the MOR and MFI zeolite. Our contributions are threefold: 1) We adapt

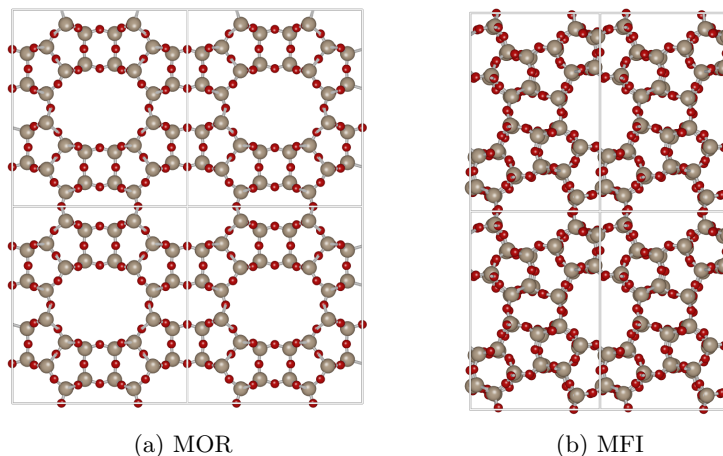(a) MOR   (b) MFI

Fig. 1: Four unit cells of all silica MOR and MFI viewed along the z-axis and y-axis respectively. Images were generated using iRASPA [7].

the Equivariant Crystal Networks (ECN) architecture from [16] to be equivariant with respect to the symmetry group of the unit cell. 2) We extend this architecture to explicitly model pores and show how this modification improves property prediction performance. 3) We introduce a new dataset containing different configurations of aluminium and silicon for the MOR and MFI zeolites, along with the CO_2 heat of adsorption values for the different configurations.

2   Related Work

Machine Learning Methods for Crystals Due to the success of different GNN architectures in modeling molecules, similar GNN architectures have been proposed for predicting material properties. Crystal Graph Convolutional Neural Networks (CGCNN) [31] are one of the first architectures for crystals, which include periodicity in the data representation and are invariant with respect to permutations of atomic indices. In the MEGNet architecture [2], a global state is used to improve the generalization of the model. Continuous filter convolutions have been introduced in the SchNet architecture [24], which as a result can model the precise relative locations of atoms better when calculating local correlations. Another approach has been proposed in DimeNet [10,11], where the network also takes directional information between atoms into account. In ALIGNN [4], the GNN processes simultaneously the graph and the line graph representation of the crystal, which takes the angles between edges into account. In addition, a transformer based architecture [32] has been proposed, which additionally encodes the periodic nature of the crystal. More recently a new approach has been proposed [16], which proposes a parameter-sharing scheme for message-passing. In this method, multiple unit cells are modelled, where parameters are shared

based on the symmetry group of the crystal lattice. As such, the model gains in expressivity by encoding a part of the crystal symmetries in its architecture.

Machine Learning in Porous Materials Existing ML methods for porous materials frequently make use of feature engineering, which is used to predict properties by traditional ML models or shallow neural networks [15,34]. Another approach made use of the CGCNN architecture [28] and extended it with engineered features [29] to improve performance. In their method, nodes in the graph representation do not correspond to atoms but rather correspond to secondary building units (SBUs), which consist of multiple atoms.

3   Crystal Symmetries

Unit Cell Zeolites are crystalline materials, meaning that they contain an infinitely repeating pattern in all directions. This pattern be described by the set of integral combinations of linearly independent lattice basis vectors $\mathbf{a_i}$:

$$\Lambda = \left\{ \sum_{i}^{3} m_i \mathbf{a}_i \mid m_i \in \mathbb{Z} \right\} \tag{1}$$

The crystal lattice has an associated translation group T_Λ, which captures translational symmetry. A unit cell is a subset of the lattice, which tiles the space of the crystal when translated by lattice vectors and is the minimum repeating pattern of the crystal. The unit cell is defined by the basis vectors as follows:

$$U = \left\{ \sum_{i}^{3} x_i \mathbf{a}_i \mid 0 \leq x_i < 1 \right\} \tag{2}$$

The unit cell of a crystalline material contains a set of atomic positions, which is defined as $S = \{\mathbf{x}_i \mid \mathbf{x}_i \in U\}$, where $\mathbf{x}_i$ is the position of the atom in the unit cell. In addition to the set of atomic positions, we also define the set of pores contained in the unit cell. We define each pore using the atoms directly surrounding the pore. We represent each pore by the location of its center, as well as its surface area along which diffusion happens in terms of Å^2. This results in the following set of pores: $P = \{(\mathbf{x}_{p_i}, area(p_i)) \mid p_i \in U\}$, where p_i is the pore and $\mathbf{x}_{p_i}$ is the centre of the pore.

Space Groups In crystalline materials, there are often multiple symmetries present inside the unit cell, defined by a space group G. The space group G is the set of isometries that maps the crystal structure onto itself. Each element of the space group can be expressed as a linear transformation $\mathbf{W}$ and a translation $\mathbf{t}$, represented by a tuple $(\mathbf{W}, \mathbf{t})$. When mapping a vector $\mathbf{x}$ using an element of the space group, it is mapped to $\mathbf{Wx} + \mathbf{t}$.

Inside a unit cell, every element of the space group G maps the atomic/pore positions in the unit cell onto itself. While the type of atom at a certain position

in the unit cell might change as a result of a transformation, the material remains the same. Therefore, each group action g of the space group can be considered a permutation of the atoms and pores in the unit cell.

Group Orbits The orbit of an element is created by applying all of the different elements of a space group G to it. If the element is a vector $\mathbf{x}$, its orbit is the set of vectors to which the element can be moved by the group action. The orbit of $\mathbf{x}$ is defined as follows:

$$G \cdot \mathbf{x} = \{g \cdot \mathbf{x} \mid g \in G\} \tag{3}$$

4 Methods

Crystal Representation In our crystal representation, we only consider the set of atoms inside of the unit cell, as the content of a unit cell fully defines the porous structures and symmetry of the material. Each atom in the unit cell is represented by a feature vector $\mathbf{t}_i$ that is a one-hot encoding of the atom type. Next to this, we represent each pore inside the unit cell with a feature vector $\mathbf{p}_i$, which contains its surface area, as well as the number of atoms surrounding it.

To represent the topology of the atoms and pores we construct a graph, where each atom is represented with a node. When the crystal contains clearly defined covalent bonds these can be used as edges in the graph, like in the case of zeolites. Pores are included in the graph representation by adding additional edges between the pore nodes and each atom on the boundary of the pore. By including these nodes, all atoms around the same pore are reachable from each other at most in two steps. Without pore nodes, this number could have been significantly larger, particularly for crystals with larger pores.

The notion of a pore has a certain analogy to the global feature vector introduced in MEGNet [2]. However, our approach is distributed in the geometry of the crystal which in turn allows the GNN-based model to learn locally distributed features, which is a more parameter-efficient solution.

Based on [24], we make use of radial basis functions to encode the distance between two neighboring nodes in the graph. We calculate the edge embedding $\mathbf{e}_{ij}$ as in Equation 4, where γ and $\boldsymbol{\mu}$ are hyperparameters. When calculating the distance between two atoms, we respect the periodic boundary conditions set by the unit cell by using the minimum image convention. Thus, we treat the opposite boundaries as a single boundary and consider the atoms and pores as neighbors and therefore sharing an edge.

$$\mathbf{e}_{ij} = \exp\left(-\gamma(\|\mathbf{x}_i - \mathbf{x}_j\| - \boldsymbol{\mu})^2\right) \tag{4}$$

Since we are developing a network architecture to predict properties based on the silicon and aluminium configuration in zeolites, we do not explicitly encode the oxygen atoms as nodes, as only the atoms placed in the T-sites of each TO_4 tetrahedron can change, while oxygen atoms always remain in the same position.

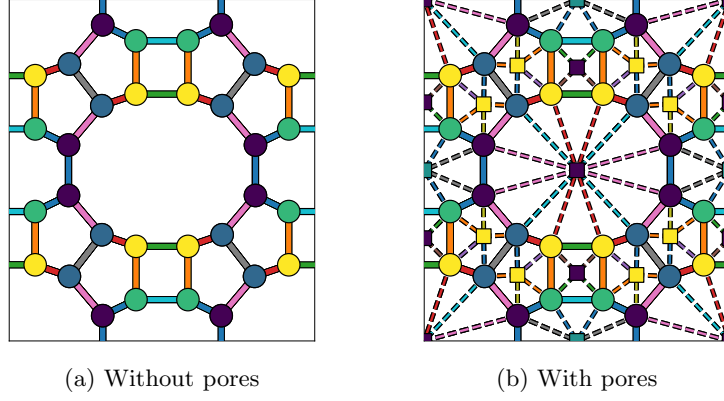(a) Without pores   (b) With pores

Fig. 2: Weight sharing scheme for MOR (z-axis). Nodes/edges of the same color share parameters in their node/edge update functions. Dashed edges are between atoms (circle) and pores (squares). Solid edges are between atoms.

Equivariant Message Passing Since the space group acts as a permutation on the atoms and pores in the unit cell, we can describe the action of a group element using Equation 5. Here, $\pi_g^{\mathbf{t}}$ and $\pi_g^{\mathbf{p}}$ are the permutations of the atoms and pores as a result of group action g.

$$\left(g\mathbf{t}_i = \mathbf{t}_{\pi_g^{\mathbf{t}}(i)} \wedge g\mathbf{p}_j = \mathbf{p}_{\pi_g^{\mathbf{p}}(j)} \right) \forall g \in G \tag{5}$$

As we model different configurations of the same crystal structure using our architecture, the model needs to be equivariant to G. The defined model is based on the message passing framework [12], which we extend by defining parameter-sharing patterns [21] for the message and node update functions.

First, we define how a parameter-sharing pattern for a graph is calculated. Following [16], we define the parameter-sharing pattern as the colored bipartite graph $\Omega \equiv (\mathbb{N}, \alpha, \beta)$. Here, $\mathbb{N}$ is the set of input atoms and pores, α is the edge color function ($\alpha : \mathbb{N} \times \mathbb{N} \to \{1, ..., C_e\}$) and β is the node color function ($\beta : \mathbb{N} \to \{1, ..., C_h\}$). C_e and C_h are the amounts of unique edge and node colors respectively. As shown in Equations 6 and 7, the color functions take the same value if two edges $((i,j), (k,l))$ or atoms/pores (i,j) lie on each other's orbit.

$$\alpha(i,j) = \alpha(k,l) \iff (k,l) \in G \cdot (i,j) \tag{6}$$
$$\beta(i) = \beta(j) \iff j \in G \cdot i \tag{7}$$

When introducing a parameter-sharing pattern based on the edge and node coloring function, we are effectively introducing an additional message (node) update function for each unique message (node) in the graph representation of the crystal. Following the proof of Claim 6.1 from [16], the model architecture remains equivariant to the space group of the crystal. In Figure 2, the parameter-sharing pattern for MOR can be found, where nodes and edges are colored according to Equations 6 and 7. The message passing operation equivariant to
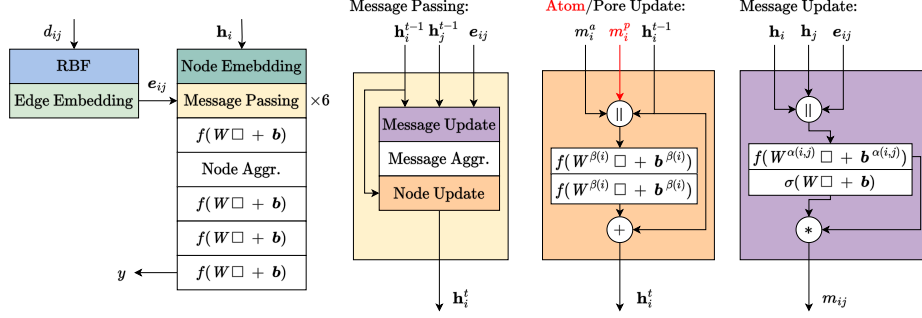
Fig. 3: Overview of the network architecture with pores. The $\square$ and $||$ denote the layer's input and concatenation respectively. The $+$ and $*$ denote elementwise summation and multiplication. $\mathbf{h}_i$ represents the embedding of node i (which can be an atom or a pore), while d_{ij} represents the distance between nodes i and j. m_i^a is the aggregated message received from atoms and m_i^p from pores. f and σ represent the leaky ReLU and sigmoid activation function respectively. $(\boldsymbol{W/b})^{\alpha(i,j)}$ and $(\boldsymbol{W/b})^{\beta(i)}$ denote the set of weights for the value of coloring functions $\alpha(i,j)$ and $\beta(i)$. In the node update function, pore nodes do not receive messages from pores (m_i^p, red). For all aggregations, sum-pooling is used. Finally, the node embedding operation is different for atom and pore nodes.

the space group is defined in Equations 8-10, where $\mathbf{t}_i$ is the atom embedding and $\mathbf{p}_i$ is the pore embedding. Here, superscript h indicates messages between atoms, k messages from pores to atoms and l messages from atoms to pores.

Since different types of crystals have different amounts of atoms and/or different space groups, we cannot share the parameters of message-passing operations between crystals. As a result, each crystal topology requires its own model.

$$\mathbf{m}_{ij}^h = \phi_e^{\alpha(i,j)}(\mathbf{t}_i^t, \mathbf{t}_j^t, \mathbf{e}_{ij}), \quad \mathbf{m}_{ij}^k = \phi_e^{\alpha(i,j)}(\mathbf{t}_i^t, \mathbf{p}_j^t, \mathbf{e}_{ij}), \quad \mathbf{m}_{ij}^l = \phi_e^{\alpha(i,j)}(\mathbf{p}_i^t, \mathbf{t}_j^t, \mathbf{e}_{ij}), \quad (8)$$

$$\mathbf{m}_i^h = \frac{1}{|N_i^h|} \sum_{j \in N_i^h} \mathbf{m}_{ij}^h, \qquad \mathbf{m}_i^k = \frac{1}{|N_i^k|} \sum_{j \in N_i^k} \mathbf{m}_{ij}^k, \qquad \mathbf{m}_i^l = \frac{1}{|N_i^l|} \sum_{j \in N_i^l} \mathbf{m}_{ij}^l, \qquad (9)$$

$$\mathbf{t}_i^{t+1} = \phi_h^{\beta(i)}(\mathbf{t}_i^t, \mathbf{m}_i^h, \mathbf{m}_i^k), \quad \mathbf{p}_i^{t+1} = \phi_h^{\beta(i)}(\mathbf{p}_i^t, \mathbf{m}_i^l). \qquad (10)$$

5 Experiments

Network Architecture In Figure 3, an overview of the model architecture is presented. First, the edges are embedded using Equation 4 on their distance (d_{ij}), which is followed by a fully connected layer. Simultaneously, both atoms and pores are embedded using two different fully connected layers, as atoms have only one feature while pores have two. In the message update function, the embeddings of the sending and receiving node and the edge embedding are concatenated, which is followed by a fully connected layer that shares weights according to Equation 6. Each message also receives a weighting factor, calculated by the fully connected layer following the equivariant layer.

The message aggregation step depends on the node type. Because pore nodes are included in the graph, we may distinguish between two types of messages based on whether they are sent from an atom or a pore. To distinguish between the origin of messages, we separately aggregate messages sent from pores (m_i^p) and atoms (m_i^a). Following the concatenation of the different messages and the node embedding, we apply 2 linear layers. The node update block also contains a residual connection [14].

Following multiple message-passing steps, the node features are sum-aggregated, and an MLP is applied to obtain the final prediction. In the model with pores, we only aggregate the pore node features. This way, we implicitly force the model to learn the contribution of each pore to the adsorption capacity.

As we are training the model on a single crystal structure at a time, it suffices to keep the architecture relatively simple. We perform 6 message passing steps, with internal hidden states of size 16. Then, we process each atom (pore) with an MLP with an output size of 24. Following this, sum-aggregation is performed, after which the final MLP makes the prediction. Our model implementation is based on ECN [16] and uses the PyTorch [20] and PyTorch scatter [8] packages as well as the AutoEquiv library [25]. The main difference with ECN is that our architecture only models one unit cell and the symmetries within it, while ECN models multiple unit cell and the symmetries between the them.
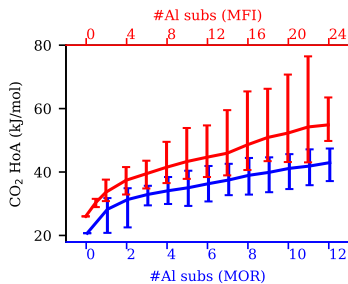

Fig. 4: Heat of Adsorption distributions per amount of Al atoms.

Data Generation To generate a dataset with porous, crystalline materials, we made use of the Mordenite and ZSM-5 zeolite frameworks. MOR contains 48 T-atoms, and adsorbates diffuse along the z-axis. MFI is a more complex zeolite, containing 96 T-atoms. It has multiple intersecting pores, where adsorbates can diffuse along the x-axis and y-axis. As a result, the adsorption capacity between two configurations with an equal amount of aluminium atoms can vary greatly.

We generated multiple MOR and MFI frameworks with varying aluminium and silicon distributions, and carried out simulations to calculate the corresponding CO_2 heat of adsorption for each configuration. For generating the structures, the Zeoran program [23] was used and atom coordinates where taken from [1]. For MOR, 4992 structures were generated, where each structure contains up to 12 aluminium atoms. For MFI, 3296 structures were generated with up to 24 aluminium atoms. The amount of aluminium atoms was chosen such that they roughly match what is possible in practice. The program makes use of four different algorithms, which places aluminium atoms in either random positions, chains, clusters or homogeneously throughout the zeolite framework. To calculate the CO_2 heat of adsorption Grand-Canonical Monte Carlo simulations were carried out using the Widom Particle Insertion method [30], performed with the

Table 2: Performance of different model architectures on CO_2 heat of adsorption prediction for the MOR and MFI datasets.

	MOR		MFI	
	MAE	MSE	MAE	MSE
CGCNN	1.374 ± 0.033	3.414 ± 0.107	2.814 ± 0.047	18.949 ± 0.561
MEGNet	1.260 ± 0.086	2.785 ± 0.290	2.674 ± 0.040	16.533 ± 0.701
Matformer	1.002 ± 0.074	1.843 ± 0.237	2.577 ± 0.372	12.552 ± 2.545
DimeNet++	0.938 ± 0.028	1.568 ± 0.076	2.862 ± 0.027	19.344 ± 0.472
SchNet	0.895 ± 0.016	1.482 ± 0.055	1.876 ± 0.047	$\mathbf{6.826 \pm 0.270}$
ALIGNN	0.828 ± 0.035	1.293 ± 0.102	$\mathbf{1.819 \pm 0.033}$	6.840 ± 0.187
ECN	1.282 ± 0.028	2.984 ± 0.124	2.484 ± 0.046	12.942 ± 0.610
Ours (w/o pores/syms)	1.184 ± 0.048	2.503 ± 0.163	2.717 ± 0.063	16.775 ± 1.093
Ours (w/o syms)	0.901 ± 0.040	1.505 ± 0.094	2.303 ± 0.110	11.841 ± 1.338
Ours (w/o pores)	0.904 ± 0.023	1.546 ± 0.075	2.029 ± 0.058	8.777 ± 0.375
Ours	$\mathbf{0.813 \pm 0.010}$	$\mathbf{1.286 \pm 0.038}$	1.902 ± 0.024	8.184 ± 0.288

RASPA software [6]. Frameworks were considered rigid and the force field parameters for the interactions between the zeolite and the adsorbate were taken from [9]. The force field for carbon dioxide was taken from [13].

In Figure 4, the 95% confidence interval of the heat of adsorption per amount of aluminium atoms is shown. While there is a strong correlation between the amount of aluminium atoms and the heat of adsorption, there is still significant variance in the heat of adsorption for each amount of aluminium substitutions.

Model Evaluation To evaluate the predictive performance of our models, we made an uninformed, random assignment of samples to the training (90%) and testing set (10%). We compare the performance of our model to different baselines [2,4,10,16,24,31,32]. For each baseline, we use the hyperparameters from their original papers. In addition, we conducted an ablation study, where we excluded pores and symmetries from our model to asses their contribution.

Since predicting the heat of adsorption is a regression task, we made use of the Huber loss function. We used the AdamW optimizer [18] with a

Table 1: Parameter count.

Model	Parameters
CGCNN	0.11M
MEGNet	0.19M
Matformer	2.77M
DimeNet++	1.74M
SchNet	0.44M
ALIGNN	4.01M
ECN	2.81M
Ours (MOR)	0.03M
Ours (MFI)	0.15M

learning rate of 0.001, and trained each model for 200 epochs. We report the mean-absolute error (MAE) and mean-squared error (MSE). To obtain confidence bounds, we trained each model 10 times with random weight initialization. The code for the model implementations and the zeolite dataset are available on `www.github.com/marko-petkovic/porousequivariantnetworks`.

As can be seen in Table 2, our model obtains the best results for MOR, and achieves competitive results with SchNet and ALIGNN on MFI, despite using

significantly fewer parameters (Table 1). In addition, our model outperformed the ablated versions. For MFI, the other baselines achieve significantly worse results. We speculate that this behaviour is caused by the spatial features of the zeolites not explicitly being encoded in the graph representation.

In Figure 5, we the true against the predicted heat of adsorption values for our best model with pores on the MOR and MFI datasets are shown. We see that most predictions for both models are accurate. For higher heat of adsorption values, the models perform slightly worse. This may be due to an insufficient amount of training examples present with a high heat of adsorption.

Fig. 5: Predicted against true heat of adsorption.

In addition, we carried out experiments to compare the data efficiency of our model, ALIGNN and SchNet. Here, we trained each model using different fractions ($\frac{1}{8}, \frac{1}{4}, \frac{1}{2}, \frac{3}{4}$ and 1) of the training set, and evaluated them on the same testing set. In Figure 6, we see that our model achieves a data efficiency comparable to ALIGNN and better than SchNet for MOR. In the case of MFI, we see that our model has a slightly lower data efficiency than ALIGNN, while performing slightly better than SchNet for low amounts of training data.
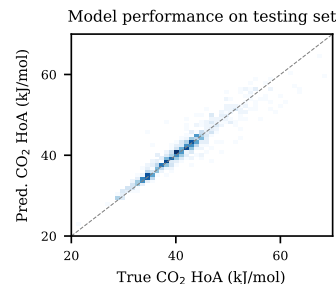
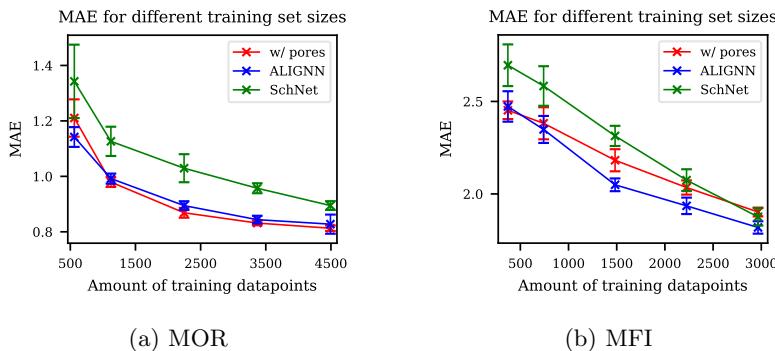

(a) MOR   (b) MFI

Fig. 6: Data efficiency (MAE on test set) with different amounts of training data.

6   Discussion

We have proposed a new type of network which can exploit both symmetries inside the unit cell as well as the structure of porous crystalline materials. Our method achieved excellent performance on the CO_2 heat of adsorption prediction task, and has also shown a better parameter efficiency and a competitive data efficiency. This class of models has a significant potential to accelerate the high throughput screening of porous materials, by quickly narrowing the search space for candidate materials.

References

1. Baerlocher, C., McCusker, L.B., Olson, D.H.: Atlas of zeolite framework types. Elsevier (2007)
2. Chen, C., Ye, W., Zuo, Y., Zheng, C., Ong, S.P.: Graph networks as a universal machine learning framework for molecules and crystals. Chemistry of Materials **31**(9), 3564–3572 (2019)
3. Choi, H.J., Jo, D., Hong, S.B.: Effect of framework si/al ratio on the adsorption mechanism of co2 on small-pore zeolites: Ii. merlinoite. Chemical Engineering Journal **446**, 137100 (2022)
4. Choudhary, K., DeCost, B.: Atomistic line graph neural network for improved materials property predictions. npj Computational Materials **7**(1), 185 (2021)
5. Choudhary, K., DeCost, B., Chen, C., Jain, A., Tavazza, F., Cohn, R., Park, C.W., Choudhary, A., Agrawal, A., Billinge, S.J., et al.: Recent advances and applications of deep learning methods in materials science. npj Computational Materials **8**(1), 59 (2022)
6. Dubbeldam, D., Calero, S., Ellis, D.E., Snurr, R.Q.: Raspa: molecular simulation software for adsorption and diffusion in flexible nanoporous materials. Molecular Simulation **42**(2), 81–101 (2016)
7. Dubbeldam, D., Calero, S., Vlugt, T.J.: iraspa: Gpu-accelerated visualization software for materials scientists. Molecular Simulation **44**(8), 653–676 (2018)
8. Fey, M.: Pytorch scatter (2023)
9. Garcia-Sanchez, A., Ania, C.O., Parra, J.B., Dubbeldam, D., Vlugt, T.J., Krishna, R., Calero, S.: Transferable force field for carbon dioxide adsorption in zeolites. The Journal of Physical Chemistry C **113**(20), 8814–8820 (2009)
10. Gasteiger, J., Giri, S., Margraf, J.T., Günnemann, S.: Fast and uncertainty-aware directional message passing for non-equilibrium molecules. In: Machine Learning for Molecules Workshop, NeurIPS (2020)
11. Gasteiger, J., Groß, J., Günnemann, S.: Directional message passing for molecular graphs. In: International Conference on Learning Representations (ICLR) (2020)
12. Gilmer, J., Schoenholz, S.S., Riley, P.F., Vinyals, O., Dahl, G.E.: Neural message passing for quantum chemistry. In: International conference on machine learning. pp. 1263–1272. PMLR (2017)
13. Harris, J.G., Yung, K.H.: Carbon dioxide's liquid-vapor coexistence curve and critical properties as predicted by a simple molecular model. The Journal of Physical Chemistry **99**(31), 12021–12024 (1995)
14. He, K., Zhang, X., Ren, S., Sun, J.: Deep residual learning for image recognition. In: Proceedings of the IEEE conference on computer vision and pattern recognition. pp. 770–778 (2016)
15. Jablonka, K.M., Ongari, D., Moosavi, S.M., Smit, B.: Big-data science in porous materials: materials genomics and machine learning. Chemical reviews **120**(16), 8066–8129 (2020)
16. Kaba, S.O., Ravanbakhsh, S.: Equivariant networks for crystal structures. In: Advances in Neural Information Processing Systems (2022)
17. Khaleque, A., Alam, M.M., Hoque, M., Mondal, S., Haider, J.B., Xu, B., Johir, M., Karmakar, A.K., Zhou, J., Ahmed, M.B., et al.: Zeolite synthesis from low-cost materials and environmental applications: A review. Environmental Advances **2**, 100019 (2020)
18. Loshchilov, I., Hutter, F.: Decoupled weight decay regularization. arXiv preprint arXiv:1711.05101 (2017)

19. Moradi, H., Azizpour, H., Bahmanyar, H., Rezamandi, N., Zahedi, P.: Effect of si/al ratio in the faujasite structure on adsorption of methane and nitrogen: a molecular dynamics study. Chemical Engineering & Technology **44**(7), 1221–1226 (2021)

20. Paszke, A., Gross, S., Massa, F., Lerer, A., Bradbury, J., Chanan, G., Killeen, T., Lin, Z., Gimelshein, N., Antiga, L., et al.: Pytorch: An imperative style, high-performance deep learning library. Advances in neural information processing systems **32** (2019)

21. Ravanbakhsh, S., Schneider, J., Poczos, B.: Equivariance through parameter-sharing. In: International conference on machine learning. pp. 2892–2901. PMLR (2017)

22. Reiser, P., Neubert, M., Eberhard, A., Torresi, L., Zhou, C., Shao, C., Metni, H., van Hoesel, C., Schopmans, H., Sommer, T., et al.: Graph neural networks for materials science and chemistry. Communications Materials **3**(1), 93 (2022)

23. Romero-Marimon, P., Gutiérrez-Sevillano, J.J., Calero, S.: Adsorption of carbon dioxide in non-löwenstein zeolites. Chemistry of Materials (2023)

24. Schütt, K., Kindermans, P.J., Sauceda Felix, H.E., Chmiela, S., Tkatchenko, A., Müller, K.R.: Schnet: A continuous-filter convolutional neural network for modeling quantum interactions. Advances in neural information processing systems **30** (2017)

25. Shakerinava, M.: Autoequiv (2 2021), `www.github.com/mshakerinava/AutoEquiv`

26. Sneddon, G., Greenaway, A., Yiu, H.H.: The potential applications of nanoporous materials for the adsorption, separation, and catalytic conversion of carbon dioxide. Advanced Energy Materials **4**(10), 1301873 (2014)

27. Stein, H.S., Gregoire, J.M.: Progress and prospects for accelerating materials science with automated and autonomous workflows. Chemical science **10**(42), 9640–9649 (2019)

28. Wang, R., Zhong, Y., Bi, L., Yang, M., Xu, D.: Accelerating discovery of metal–organic frameworks for methane adsorption with hierarchical screening and deep learning. ACS Applied Materials & Interfaces **12**(47), 52797–52807 (2020)

29. Wang, R., Zou, Y., Zhang, C., Wang, X., Yang, M., Xu, D.: Combining crystal graphs and domain knowledge in machine learning to predict metal-organic frameworks performance in methane adsorption. Microporous and Mesoporous Materials **331**, 111666 (2022)

30. Widom, B.: Some topics in the theory of fluids. The Journal of Chemical Physics **39**(11), 2808–2812 (1963)

31. Xie, T., Grossman, J.C.: Crystal graph convolutional neural networks for an accurate and interpretable prediction of material properties. Physical review letters **120**(14), 145301 (2018)

32. Yan, K., Liu, Y., Lin, Y., Ji, S.: Periodic graph transformers for crystal material property prediction. Advances in Neural Information Processing Systems **35**, 15066–15080 (2022)

33. Yang, C.T., Janda, A., Bell, A.T., Lin, L.C.: Atomistic investigations of the effects of si/al ratio and al distribution on the adsorption selectivity of n-alkanes in brønsted-acid zeolites. The Journal of Physical Chemistry C **122**(17), 9397–9410 (2018)

34. Zhang, C., Xie, Y., Xie, C., Dong, H., Zhang, L., Lin, J.: Accelerated discovery of porous materials for carbon capture by machine learning: A review. MRS Bulletin **47**(4), 432–439 (2022)